RESEARCH ARTICLE

Two-Stage Stochastic Optimal Power Flow for Microgrids With Uncertain Wildfire Effects

SIFAT CHOWDHURY AND **YU ZHANG**, (Member, IEEE)

Department of Electrical and Computer Engineering, University of California, Santa Cruz, CA 95064, USA

Corresponding author: Yu Zhang (yzhan419@ucsc.edu)

ABSTRACT Large-scale power outages caused by extreme weather events are one of the major factors weakening grid resilience. In order to prevent the critical infrastructure from cascading failure, power lines are often proactively de-energized under the threat of a progressing wildfire. In this context, the potential of microgrid (MG) functioning in islanded mode can be exploited to enhance the resiliency of the power grid. However, there are numerous uncertainties originating from these types of events and an accurate modeling of the MG is required to harness its full potential. In this paper, we consider the uncertainty in line outages depending on fire propagation and reduced solar power generation due to the particulate matter in wildfire smoke. We formulate a two-stage stochastic MG optimal power flow problem by utilizing a second-order cone relaxation of the DistFlow model. Leveraging an effective approximation of the resistive heat gain, we separate the complicating constraints of dynamic line rating from the resulting optimization problem. Extensive simulation results corroborate the merits of our proposed framework, which is tested on a modified IEEE 22-bus system.

INDEX TERMS Extreme weather events, microgrid energy management, stochastic optimization, wildfire smoke effect.

NOMENCLATURE

Sets and Indices

$\mathcal{N}^{ES}/\mathcal{N}^{MS}$	Set of all buses having energy storage systems (ES) / mobile ES(MS).
$\mathcal{N}^{L}/\mathcal{N}^{QS}$	Set of all load bus/ buses equipped with emergency generators or quick start (QS) units.
$\mathcal{N}^{MT}/\mathcal{N}^{PV}/\mathcal{N}^{WT}$	Set of all buses connected with micro-turbines (MT) / PV cells / wind turbines (WT).
$\mathcal{S}/\mathcal{T}$	Set of all scenarios / Set of hours for second stage variables $\mathcal{T} \triangleq \{1, 2, \ldots, T\}$.
$i, j/ij$	Indices for buses/Distribution line between i and j.
t/s	Index of hours / Index for scenarios.

T'	Look ahead window for first stage variables.

Parameters

$\bar{\ell}_{ij}$	Maximum squared magnitude of current flowing through line ij.
$\bar{N}^{MS}/\bar{C}^{MS}$	Maximum number/allocated budget for MS units.
$\bar{P}^{B}/\bar{P}^{S}$	Maximum amount of power to be bought from/sold to the upstream network (MW).
$\bar{P}^{ES,ch}/\bar{P}^{ES,dis}/$ $\bar{P}^{MS,ch}/\bar{P}^{MS,ch}$	Upper limit of ES/ MS charging/discharging power (MW).
$\bar{P}^{MT}$	MT maximum power output (MW).
$\bar{X}$	Maximum amount of fuel reserve that can be bought.
$\bar{Y}^{\delta}/\underline{Y}^{\delta}$	Upper/lower limit of QS fuel expenditure.
β/ϵ	Load criticality factor / Solar absorptivity.

$\eta^{\text{ch}}/\eta^{\text{dis}}$	ESS charging/discharging efficiency.	$q^{\text{s}}/q^{\text{f}}$	Radiative heat gain rate from solar/fire (W/m).
η^{QS}	Conversion factor of QS fuel expenditure and power output.	q^{l}	Resistive heat gain rate (W/m).
γ^{L}	Incentive for serving per unit of load ($/MW).	$q^{\text{r}}/q^{\text{c}}$	Radiative/Convective heat loss rate (W/m).
γ^{MS}	Transportation cost of carrying an MS unit ($).	T_{ij}	Temperature of conductor connecting bus i and j (K).
$\gamma^{\text{MT}}/\gamma^{\text{QS}}$	Marginal cost of active power generation from MT/QS units ($/MW).	u_{ij}	Binary variable indicating line outage status.

Decision Variables

γ^{RF}	Price for buying per unit of renewable fuel ($/L).	$\alpha^{\text{ls}}/\alpha^{\text{ch}}/\alpha^{\text{dis}}$	Ratio of the served load to its actual demand/binary indicator for charging/discharging status for MS units.
κ^{a}	Absolute viscosity of air (kg/ms).		
κ_{B}	Stefan-Boltzmann constant (W/m^2/K^4).		
μ^{a}	Thermal conductivity of air (W/mK).	ℓ_{ij}	Squared magnitude of current flowing through line ij.
$\Phi^{\text{s}}/T_{\text{f}}$	Solar radiation (W/m^2) /Flame zone temperature (K).	$P^{\text{ES,ch}}/P^{\text{ES,dis}}$ $/P^{\text{MS,ch}}/P^{\text{MS,dis}}$	Scheduled ES/MS charging/ discharging active power (MW).
π_s	Probability of each scenario.		
ψ^{w}	Angle between wind direction and conductor(rad).	P_{ij}/Q_{ij}	Active/reactive power flow through branch ij (MW/MVar).
$\rho^{\text{a}}/\rho^{\text{b}}$	Air density / Density of bulk fuel (kg/m^3).	P_i/Q_i	Active/reactive power injection at bus i (MW/MVar).
$\sigma^{\text{f}}/\sigma^{\text{c}}$	Emissivity of flame zone / conductor (dimensionless).	$S_i^{\text{S}}/S_i^{\text{M}}$	State of charge of the i-th ES/MS unit.
τ^{a}	Atmospheric transmissivity (dimensionless).	v_i	Squared voltage magnitude at bus i.
ϱ/H	Conductor diameter/Flame height (m).	X_i/Y_i	Renewable fuel reserve / Remaining fuel of the i-th QS unit.
$\vartheta^{\text{w}}/\varphi$	Wind speed (m/sec) / Flame tilt angle (rad).		
ζ	Thermal resistivity coefficient of the conductor (K^{-1}).	Z_i	Binary indicator whether an MS unit is sited at bus i.
C_p	Relative heat capacity (J/kg/K).		
F	Effort level for extinguishing fire (dimensionless).		
k_p/k_v	Droop constants.		
M	Indicator for uphill (0) and downhill (1).		
N	Indicator for presence (10) or absence (0) of nearby natural obstacles.		
$P^{\text{L}}/Q^{\text{L}}$	Active/reactive power demand (MW/MVar).		
$P^{\text{MT,ru}}/P^{\text{MT,rd}}$	MT ramping up/down limit (MW).		
r_{ij}/x_{ij}	Line resistance/reactance between bus i and bus j (Ω).		

Scenario Generation Variables

$\check{T}/\vartheta^{\text{f}}$	Ambient temperature (K) / Fire spread rate(m/sec).
Φ^{f}	Radiative heat flux emitted from wildfire (W/m^2).
θ^{f}	View angle between the flame and the conductor (rad).
d^{f}	Distance between fire and power line (m).

I. INTRODUCTION

Extreme weather events pose a great threat to the system planning and operation of electrical grids. They severely affect the reliability and resiliency of the power system by damaging critical infrastructure like power lines and other electrical equipment. This leads to prolonged power outages to a large customer base and critical loads in the system. According to the U.S. Energy Information Administration, customers faced over eight hours of power interruption on average in 2020, which has doubled in just five years [1]. More frequent power outages due to high-impact, low-probability events result in tremendous financial losses, roughly $150 billion per year [2]. As one of the most devastating natural disasters, wildfires take a toll on human beings and the environment by emitting tons of greenhouse gases. Moreover, to reduce the risk of power line induced fires, frequent public safety power shutoffs (PSPS) also cause huge economic losses. The disrupted power supply caused by a wildfire can be overcome by deploying microgrids (MG). A big advantage of a MG is that it can perform as an independent entity to serve its load when getting disconnected from the main grid. On top of that, MG makes the grid

greener and more sustainable by integrating distributed energy resources (DER), including the microturbine (MT), renewable energy from photovoltaic (PV) panels, and wind turbines (WT).

A. MOTIVATION

The optimal operation of a MG during a wildfire is subject to several uncertain factors. First of all, the progression of the fire and its degree of devastation depends upon a lot of features, including but not limited to wind speed, wind direction, and the amount of flammable fuel in the surrounding area. The onset of any contingency in the electric distribution system depends upon the fire dynamics. Furthermore, the generation portfolio of PV and WT is inherently stochastic, unlike conventional generators. During a wildfire, aerosols produced by the burning of organic substances visibly block sunlight from reaching the earth's surface and make the atmosphere darker. Therefore, the output from PV panel drops down due to the presence of smoke and soot containing different airborne particulate matter. According to California Independent System Operator (CAISO), the solar powered electricity generation declined more than 30% in the first half of September 2020 in just 2 months when the state was experiencing one of the biggest fires in its history [3]. Similarly, the power output from WT and the load consumption profile of the customers are also contingent upon different scenarios. Therefore, these components need to be analyzed carefully to ensure the optimal scheduling of a MG.

B. LITERATURE REVIEW

Ensuring power supply to customers threatened by wildfire risks is a highly multi-disciplinary field of research encompassing geography, meteorology, engineering, and resource management. From a holistic point of view, we break down this broad topic into several key aspects as presented in Table 1. Predicting an extreme weather event is the first step to dealing with the adverse effects it takes along. To get off the ground, an effective model for wildfire prediction is essential to estimate the chance of a fire-induced power outage in a region. Authors from [4], [5], [6], and [7] investigate the underlying factors e.g. temperature, humidity, wind speed, vegetation condition, and topology that can initiate a fire. However, these works do not comprise a fire propagation model through which the risk and scale of an imminent fire can be determined. To overcome this challenge, [8] and [9] incorporate wildfire dynamics in their model for determining line outage by a progressing fire and achieving an optimal distribution system operation. A spatiotemporal fire monitoring technique in combination with a decision support tool for fire management is used by [10] in order to mitigate the impacts of wildfires on the power grid. Dian et al. design a framework by integrating a prediction model and line outage probability to get an early warning of disrupted power lines [11]. Nonetheless, their efforts are limited by

strong assumptions, complicated problem formulation, and the absence of fire-extinguishing efforts.

Apart from the necessity of having dynamic wildfire prediction models, the energy management of a MG in a high fire risk zone is challenged by numerous uncertainties such as repair time of damaged equipment, islanded status, and intermittent renewable generation. Reference [12] co-optimizes system operation and repair crew routing considering the uncertainty in repair time and load demand. A stochastic optimization framework is developed for scheduling resources considering the uncertain duration of islanded operation of MG in [13] and [14]. While their effort is important for the optimal operation of the power network, however, there are missing factors like fire extinguishing works that can alter the duration of the islanded condition.

Renewable energy resources such as PV panels and WT are one of the key distributed generation components in MG which are inherently stochastic. The survey [15] covers the recent advancements in stochastic optimization for modeling the uncertainties in renewable energy applications. The stochasticity of these resources is further captured through a robust optimization-based model in [16] and [17], by an approximate dynamic programming-based approach in [18] and as a security-constrained stochastic framework for the economic dispatch of flexible resources in [19]. Besides, several data-driven models are also proposed to approximate the uncertain sets originated by high penetration of renewable energy and load in [20], using a hierarchical hybrid control method [21], distributionally robust approach [22] and an adaptive robust formulation [23]. Although these works significantly enhance the efficiency of renewable energy based models, nevertheless, they lack in assessing the adverse effects on solar power generation stemming from the fire smoke. Few works exist in the literature exploring the smoke effect by analyzing different molecules and particles produced by smoke [24], [25]. Reference [26] develop a model to estimate the power output reduction on different PV cell technologies. Using the optical properties of smoke and the spectral response of PV cell materials, an estimated PV power reduction approach is presented in [27]. Due to this sudden drop in power generation, [28] studies the frequency stability on the power grid. Despite all, there remains a research gap in arranging a compensation strategy for the likely unserved loads during blackouts caused by the reduced generation.

Other diverse initiatives to make the power grid resilient against disasters are extensively studied in the literature. Public safety power shut-off is one of the emergency measures where electric components are selectively de-energized to reduce the risk of fire ignition. This task is formulated by [29] and [30] to minimize the risk of fire ignition from grid fault and maximize secure power delivery. Besides that, researchers also develop strategies for restoring loads during a natural disaster. Reference [31] coordinates mobile resources, multiple generating units, and demand response, thus balancing the supply and demand side for restoring

TABLE 1. Summary of the literature review.

Topic	References	Contribution	Limitation
Wildfire prediction	[4], [5], [6], [7]	Analysis of meteorological factors causing wildfires	Lacks fire dynamics
Fire propagation model	[8], [9], [11], [10]	Determining line outage by tracking fire progression	• DLR constraints coupled to optimization problem • Absence of human and natural intervention • Line outage being considered for tie-line only
Uncertainty modelling • Islanding duration • Renewable energy generation	[13], [14] [21], [22], [18], [19], [23], [16], [17]	• The onset and duration of islanding mode • Addressing the inherent stochastic nature of energy	• Absence of fire extinguishing efforts • Absence of factors altering the predicted generation due to fire
Smoke effect	[24], [25], [43], [26], [28], [27]	Analysis of particulate materials present in smoke	Compensating the reduced solar power generation for serving loads
Resilience initiatives • PSPS • Load restoration • Resource allocation	[29], [30] [31], [34] [35], [38]	• Reducing risks of fire ignition from power cables • Restoring curtailed loads • Pre-event preparation for securing additional resources	• Load curtailment • Void of modelling and impacts of disasters on the distribution network • Over estimation due to ignoring disaster-induced reduction of renewable energy generation

loads. Another collaborative strategy between network reconfiguration and spatiotemporal distribution of EV is explored in [32] while [33] simultaneously combines the repair process of the distribution system and load restoration problem. Network configuration is another way of serving critical loads affected by a natural disaster. An advanced configuration of the distribution system is presented for restoring such loads [34].

Besides, securing additional resources is another good practice that helps in overcoming the service disruption caused by an extreme weather event. From a resource allocation perspective, researchers propose a stochastic mixed integer linear programming model consisting of mobile and labor resources to assist load restoration in the post-event phase [35]. By forming adaptive multi microgrids with mobile energy resources [36], topology switching [37], resilience against extreme conditions is achieved. Besides, Lie et al formulate security constraints for spinning and non-spinning reserves in a limited energy resources setup against contingencies [38]. Moreover, there are efforts in advancing novel techniques to solve the energy management problem involving MG. A combination of two-stage stochastic programming and model predictive control is applied for MG energy management under uncertainties [39], [40]. A quantum teaching learning-based algorithm is also proposed by [41] that captures the seasonal variation of solar and wind power generation. Furthermore, demand response is incorporated in optimal energy dispatch strategies that potentially can decrease MG operation cost; see [42]. One key shortcoming of these works is to disregard the uncertain effects of line outage caused by a progressing fire and smoke induced reduction in PV generation. Because of these effects, load service gets disrupted, which eventually affects the reliability and resilience of the power grid.

C. OUR CONTRIBUTIONS
In this work, we propose a MG scheduling task by formulating a two-stage stochastic optimal power flow (OPF) problem considering two significant effects induced by an approaching wildfire, namely line outage and smoke-altered PV generation. We make reasonable assumptions to convexify the original non-convex problem and reduce computational complexity. The proposed framework is tested through extensive simulation to demonstrate the system's resilience compared with some existing schemes. The novelty and contributions of our work are summarized as follows:
- We comprehensively model wildfire propagation by incorporating natural and human exertion on top of meteorological and geographical factors. The inclusion of these factors captures both the progress and deflection of the fire front, which determines probable line outages.
- We model the curtailed PV generation originating from fire smoke using a data-driven approach. We assess the requirement of securing additional reserves to compensate for this shortage of generation. This ensures maximum load supply during service interruption.
- We introduce a simple but effective approximation of the resistive heat gain rate, which facilitates the separation of the dynamic line rating constraints from the optimization problem. It helps in the convexification of the original problem and significantly reduces the computational burden.

The rest of this paper is organized as follows. Section II describes the system modeling consisting of the wildfire dynamics and smoke effect. In Section III, the formulation of a two-stage stochastic optimization problem is discussed. Simulation studies are presented in Section IV. Finally, Section V provides the concluding remark along with the future research direction.

II. SYSTEM MODELING

A. SCENARIO GENERATION

The uncertainties regarding the progression of wildfire and renewable generation are incorporated in our model as different scenarios. The stochastic parameters for these scenarios are wind speed (ϑ^{w}), wind direction (ψ^{w}) and solar radiation (Φ^{s}). Each of them is modeled respectively by the Weibull, von Mises and Beta distribution function using historical data for each hour of the day. The other parameters considered are firefighting efforts, natural barriers, and regional topography as described in (1a). Afterward, sufficient scenarios consisting of variables (listed earlier in the nomenclature section for scenario generation) as functions of these parameters are generated for 24 hours of a day using Monte Carlo simulation. The output power from the WT is calculated as mentioned in [44]. For the remaining parts of this paper, the subscripts $\{ij, s, t\}$ stand for the line connecting bus i and j at time t for scenario s.

B. WILDFIRE MODELLING

To incorporate the fire dynamics in our modeling, we leverage a classic heat flux model [45]. One of the limitations of this model is that it considers neither the human or natural intervention decelerating fire spread nor the impact of the topography of a region. To overcome this, our proposed fire propagation model is given as follows.

$$\vartheta^{f}_{s,t} = 0.07 \times \frac{(1 + \vartheta^{w}_{s,t})}{\rho^{b}} \times e^{-F} \times e^{-N} \times e^{-1^{M} \times |\text{slope}|}$$

$$\text{(1a)}$$

$$d^{f}_{ij,s,t} = d^{f}_{ij,s,t-1} - \vartheta^{f}_{s,t} \Delta t \cos(\psi^{w}_{ij,s,t}) \qquad \text{(1b)}$$

$$\theta^{f}_{ij,s,t} = \arctan\left(\frac{H\cos(\varphi)}{d^{f}_{ij,s,t} - H\sin(\varphi)}\right) \qquad \text{(1c)}$$

$$\Phi^{f}_{ij,s,t} = 0.5 \times \sigma^{f}\kappa_{B}\tau^{a}T^{4}_{f}\sin(\theta^{f}_{ij,s,t}). \qquad \text{(1d)}$$

First, in (1a), the fire spread rate ϑ^{f} is expressed as a function of wind speed ϑ^{w}, bulk fuel density ρ^{b}, natural and human fire fighting efforts and the type of topography. Fuel density indicates the vegetation level of the area. We model the human firefighting factor as an exponential function where F quantifies different levels of effort. The rationale behind this modeling is that the growth or decay of any object is naturally modeled as an exponential function. F can take three distinct values respectively, indicating no effort, moderate effort (use of fire hose from ground level), and extensive effort (combination of fire hose from ground and water planes from above. The next term (N) indicates the presence of natural barriers like water bodies and rocky outcrops that hinder fire growth. The last term (M) in this equation is the contributing factor by the landscape of an area [11]. M can be either 0 or 1, standing for uphill and downhill, respectively. Fire spreads faster on slanted land compared to flat land. Moreover, in the uphill, the radiant heat from the wildfire pre-heat fuels on the slope ahead of the fire-front which aids in faster propagation than in downhill. Afterward, (1b) reflects the dynamics of the

distance, d^{f} between fire and the power line connecting bus i and j based on the wind speed and direction. Then, the view angle θ^{f} is calculated according to (1c), which depends on the distance d^{f}, flame height H and flame tilt angle φ. Finally, we obtain the radiative heat flux Φ^{f}_{ij} emitted from the fire to the power line, as shown in (1d).

C. DYNAMIC LINE RATING (DLR)

The temperature of an overhead conductor (power distribution line) is constantly changing in response to changes in weather conditions and the current flowing through it. In this subsection, we study the impact of the nearby fire and other factors on the conductor's temperature according to the IEEE standard 738-2012 [46].

The dynamics of the line temperature $T_{ij,s,t}$ are quantified in heat balance equation (2a), where three heat gain sources, respective from fire, solar and line current $\{q^{f}, q^{s}, q^{l}\}_{ij,s,t}$ and two heat loss sources through radiation and convection $\{q^{r}, q^{c}\}_{ij,s,t}$ are modeled by equations (2c)-(2g). As shown in the *big-M* constraint (2b), if T_{ij} exceeds the maximum permissible temperature $\bar{T}_{ij}$, this line is switched off ($u_{ij} = 0$) to ensure safe operation.

$$T_{ij,s,t+1} - T_{ij,s,t}$$
$$= \frac{\Delta t}{mC_{p}} \times \left(q^{f}_{ij,s,t} + q^{s}_{ij,s,t} + q^{l}_{ij,s,t} - q^{r}_{ij,s,t} - q^{c}_{ij,s,t}\right)$$

$$\text{(2a)}$$

$$T_{ij,s,t} \leq \bar{T}_{ij} + \left(1 - u_{ij,s,t}\right) \times M \qquad \text{(2b)}$$

$$q^{f}_{ij,s,t} = \varrho_{ij}\Phi^{f}_{ij,s,t} \qquad \text{(2c)}$$

$$q^{s}_{ij,s,t} = \varrho_{ij}\epsilon_{ij}\Phi^{s}_{ij,s,t} \qquad \text{(2d)}$$

$$q^{l}_{ij,s,t} = R_{ij,s,t}(T_{ij,s,t}) \times \ell_{ij,s,t} \qquad \text{(2e)}$$

$$q^{r}_{ij,s,t} = 1.78 \times 10^{-7} \times \varrho_{ij} \times \sigma^{c} \times (T^{4}_{ij,s,t} - \check{T}^{4}_{ij,s,t}) \qquad \text{(2f)}$$

$$q^{c}_{ij,s,t} = \mu^{a}\chi_{ij,s,t} \times (T_{ij,s,t} - \check{T}_{ij,s,t}) \times f(\text{Re}_{ij,s,t}) \qquad \text{(2g)}$$

where in (2e) and (2g) we have

$$R_{ij,s,t}(T_{ij,s,t}) = R^{\text{ref}}_{ij} \times \left(1 + \zeta_{ij} \times (T_{ij,s,t} - T^{\text{ref}}_{ij})\right)$$

$$\text{Re}_{ij,s,t} = \frac{\varrho_{ij}\rho^{a}\vartheta^{w}_{s,t}}{\kappa^{a}}$$

$$f(\text{Re}_{ij,s,t}) = \max\left\{1.01 + 1.35 \times \text{Re}^{0.52}_{ij,s,t},\ 0.754 \times \text{Re}^{0.6}_{ij,s,t}\right\}$$

$$\chi_{ij,s,t} = 1.194 + 0.194 \times \cos(2\psi^{w}_{ij,s,t})$$
$$+ 0.368 \times \sin(2\psi^{w}_{ij,s,t}) - \cos(\psi^{w}_{ij,s,t}).$$

D. SMOKE EFFECT

Solar panels produce energy by absorbing sunlight passing through the atmosphere. The total solar irradiance emitted from the sun is termed as global horizontal irradiance (GHI). However, the output from a solar panel depends upon a fraction of GHI that incidents perpendicularly on the solar panel, namely direct normal irradiance (DNI). The rest of the GHI is diffused by different molecules and particles in the atmosphere and contributes little to the PV generation. Wildfire smoke can severely affect the PV generation

capacity by blocking the effective solar irradiance. The presence of particulate matter (PM), specifically PM2.5 and PM10 in the smoke plume mainly affects PV production while clouds and some other meteorological parameters contribute there too. The atmospheric clouds reflect and scatter the sunlight and prevent them from reaching the PV panels. Hence, the thicker the cloud is, the less the power generation will be. Similarly, the higher concentration of PM attenuates PV output. Moreover, a higher relative humidity indicates the presence of more water vapor in the atmosphere, which causes more refraction and reflection of direct insolation of sunlight.

In [43] the effect of a short-span prescribed fire burn on solar irradiance and PV power was investigated. There was no conclusive correlation among the factors causing the PV output reduction. Reference [25] studied the effect of aerosol on surface solar radiation considering a clear sky condition. Reference [8] used Beta distribution to model the GHI while ignoring crucial factors such as the existence of airborne PM caused by a fire. Without considering the cloud and all types of PM, [24] measured the effect of certain environmental factors causing a reduced PV generation. Hence, during a contingency, the PV generation forecast can be highly overestimated. Moreover, a theoretical model was developed by [27] to estimate the PV output reduction by using the optical properties of smoke. The impact on frequency stability arising from this sudden reduction in generation on the power grid was analyzed by [28]. Reference [26] developed another data-driven model to study how solar power reduction varies in different PV cell technologies.

To this end, in order to quantify the smoke effect more accurately, we postulate the following multivariate regression model:

$$P_{s,t}^{\mathrm{PV}} = \alpha_0 + \alpha_1 Z_1 + \alpha_2 Z_2 + \alpha_3 Z_3 + \alpha_4 Z_4 \\ + \alpha_5 \ln(Z_5) + \alpha_6 \ln(Z_6), \quad (3)$$

where the target value is the measured PV generation output P^{PV}. The features include temperature Z_1, relative humidity Z_2, DNI on the PV panel Z_3, cloud opacity Z_4, the concentrations of PM2.5 Z_5 and PM10 Z_6. For the last two factors, natural logarithm is applied because the solar irradiation changes exponentially with the presence of the particulate matter. Z_3 is the net solar irradiation reaching the PV panels, which is equal to the DNI multiplied by the cosine of solar zenith angle θ_z. All the variables are standardized by subtracting their mean values and divided by the standard deviations.

III. PROBLEM FORMULATION
We represent a MG as a directed tree graph $\mathcal{G} \triangleq (\mathcal{N}, \mathcal{E})$, where $\mathcal{N}$ is the set of buses and $\mathcal{E}$ denotes the set of power lines (branches). We assume that buses can either be connected with a load, microturbines (MT), quick start generators (QS), wind turbines (WT) or PV panels. In addition, all PV and WT buses are equipped with energy storage systems (ES) and a mobile energy storage (MS) unit

can be sited to any bus other than the load buses. Therefore, we have $\mathcal{N} = \mathcal{N}^{\mathrm{L}} \cup \mathcal{N}^{\mathrm{MT}} \cup \mathcal{N}^{\mathrm{QS}} \cup \mathcal{N}^{\mathrm{PV}} \cup \mathcal{N}^{\mathrm{WT}}$, $\mathcal{N}^{\mathrm{ES}} = \mathcal{N}^{\mathrm{PV}} \cup \mathcal{N}^{\mathrm{WT}}$ and $\mathcal{N}^{\mathrm{MS}} = \mathcal{N} \setminus \mathcal{N}^{\mathrm{L}}$. Unless specified otherwise, the objective function and constraints described in this section hold for all scenarios $s \in \mathcal{S}$.

A. OBJECTIVE FUNCTION
Considering the inherent uncertainty of renewable energy generation and wildfire dynamics, we formulate the task of MG optimal power scheduling as a two-stage stochastic optimization problem. The objective function (4) minimizes the costs of power generation and load curtailment that occurred in the first and second stages. The total time horizon is divided into two segments, T' and $\mathcal{T}$ which respectively realize the first and second stage variables. The first stage variables include siting an MS unit $\{Z_i\}_{i \in \mathcal{N} \setminus \mathcal{N}^{\mathrm{L}}}$ to bus i and the allocated fuel reserves $\{X_i\}_{i \in \mathcal{N}^{\mathrm{QS}}}$ for the QS generators. Then, we generate a sufficiently large number of scenarios consisting of various fire dynamics, weather conditions and the smoke effect. In the second stage, the goal is to minimize the total expected operation cost while maximizing prioritized load serving. The variables include real-time dispatch commands and other network operational variables in the MG.

$$\text{minimize } C_1 \left(\{Z_i, X_i\}_i \right) + C_2 \left(\{P_{i,s,t}, \alpha_{i,s,t}^{\mathrm{ls}}\}_{i,s,t} \right) \quad (4)$$

where

$$C_1 \left(\{Z_i, X_i\}_i \right) = \sum_{i \in \mathcal{N} \setminus \mathcal{N}^{\mathrm{L}}} \gamma^{\mathrm{MS}} Z_i + \sum_{i \in \mathcal{N}^{\mathrm{QS}}} \gamma^{\mathrm{RF}} X_i \quad (5a)$$

$$C_2 \left(\{P_{i,s,t}, \alpha_{i,s,t}^{\mathrm{ls}}\}_{i,s,t} \right) = \sum_{s \in \mathcal{S}} \sum_{t \in \mathcal{T}} \pi_s \times \Bigg(\sum_{i \in \mathcal{N}^{\mathrm{QS}}} \gamma^{\mathrm{QS}} P_{i,s,t} \\ + \sum_{i \in \mathcal{N}^{\mathrm{MT}}} \gamma^{\mathrm{MT}} P_{i,s,t} \\ - \sum_{i \in \mathcal{N}^{\mathrm{L}}} \gamma^{\mathrm{L}} \alpha_{i,s,t}^{\mathrm{ls}} \beta_{i,t} P_{i,s,t}^{\mathrm{L}} \Bigg) \quad (5b)$$

The term $\alpha_{i,t,s}^{\mathrm{ls}} \beta_{i,t} P_{i,t}^{\mathrm{L}}$ reflects the prioritized load serving amount. In order to prioritize demand satisfaction, the incentive for serving loads is set large enough.

B. FIRST STAGE CONSTRAINTS
The variables in this stage are decided T' hours before the second stage scheduling begins. The siting of MS units is constrained by the number of units and the potential budget allocated for them. (6a) and (6b) denote these constraints. For simplicity, we assume that all the units are of the same size, fully charged and each bus can accommodate only one MS unit. (6c) limits the summation of the total amount of renewable fuel reserve that can be allocated to all QS units, $i \in \mathcal{N}^{\mathrm{QS}}$.

$$\sum_{i \in \mathcal{N} \setminus \mathcal{N}^{\mathrm{L}}} Z_i \leq \bar{N}^{\mathrm{MS}} \quad (6a)$$

$$\sum_{i \in \mathcal{N} \setminus \mathcal{N}^{\mathrm{L}}} \gamma^{\mathrm{MS}} Z_i \leq \bar{C}^{\mathrm{MS}} \tag{6b}$$

$$0 \leq \sum_{i \in \mathcal{N}^{\mathrm{QS}}} X_i \leq \bar{X}. \tag{6c}$$

C. SECOND STAGE CONSTRAINTS

This subsection explains the operational constraints of the MG for all time $t \in \mathcal{T}$.

1) POWER FLOW CONSTRAINTS

For $j \in \mathcal{N}$ and $(i, j) \in \mathcal{E}$, an SOCP relaxation of the *DistFlow model* (7a)-(7d) is adopted to quantify the power flows in the radial network; see e.g., [47]. Furthermore, (7e)-(7f) set the lower and upper limits for the nodal voltages and branch currents to ensure safe operation. The voltage of the reference bus is also fixed at 1 p.u.

$$P_{j,s,t} = \sum_{k:j \to k} P_{jk,s,t} - \sum_{i:i \to j} \left(P_{ij,s,t} - r_{ij}\ell_{ij,s,t} \right) \tag{7a}$$

$$Q_{j,s,t} = \sum_{k:j \to k} Q_{jk,s,t} - \sum_{i:i \to j} \left(Q_{ij,s,t} - x_{ij}\ell_{ij,s,t} \right) \tag{7b}$$

$$v_{j,s,t} = v_{i,s,t} - 2 \left(r_{ij}P_{ij,s,t} + x_{ij}Q_{ij,s,t} \right) + (r_{ij}^2 + x_{ij}^2)\ell_{ij,s,t} \tag{7c}$$

$$P_{ij,s,t}^2 + Q_{ij,s,t}^2 \leq \ell_{ij,s,t} v_{j,s,t} \tag{7d}$$

$$\underline{v} \leq v_{j,s,t} \leq \bar{v}, \quad v_{s,t}^{\mathrm{ref}} = 1. \tag{7e}$$

$$0 \leq \ell_{ij,s,t} \leq \bar{\ell}_{ij} \tag{7f}$$

2) REACTIVE POWER CONSTRAINTS

We assume that all the buses except for the load bus are equipped with controllable inverters. Hence, reactive power constraints are given as

$$|Q_{i,s,t}| \leq \bar{Q}_i, \quad \forall i \in \mathcal{N} \setminus \mathcal{N}^{\mathrm{L}}. \tag{8}$$

3) QS CONSTRAINTS

To be environmentally friendly and cost effective, the MG leverages renewable fuels for quick start (QS) units as non-spinning reserves to restore the loads after an islanding event with PSPS. The following constraints hold for all $i \in \mathcal{N}^{\mathrm{QS}}$. $Y_{i,s,t}$ is the remaining fuel in the i-th QS unit. (9a) sets the initial fuel remaining in the i-th unit as the amount of fuel allocated to that unit in the first stage. This is a coupling constraint between the first and second stages. (9b) ensures that these units only start to operate at the next time step after any of the lines gets tripped off together with a limit for ramping up and down of the fuel expenditure (9c) relates the fuel expenditure with the amount of power produced with a conversion factor η^{QS}. (9d) represents the non-negativity constraints for the remaining fuel level and power output, respectively.

$$Y_{i,s}^{\mathrm{int}} = X_i \tag{9a}$$

$$\prod_{ij \in \mathcal{E}} (1 - u_{ij,s,t}) \times \underline{Y}_i^\delta \leq Y_{i,s,t} - Y_{i,s,t+1}$$
$$\leq \prod_{ij \in \mathcal{E}} (1 - u_{ij,s,t}) \times \bar{Y}_i^\delta, \quad \forall t \in \mathcal{T} \setminus \{T\} \tag{9b}$$

$$P_{i,s,t+1} = \eta^{\mathrm{QS}} \times (Y_{i,s,t} - Y_{i,s,t+1}), \quad \forall t \in \mathcal{T} \setminus \{T\} \tag{9c}$$

$$Y_{i,s,t} \geq 0, P_{i,s,t} \geq 0 \tag{9d}$$

4) MT CONSTRAINTS

The generation limits and ramping up/down constraints for each MT unit at node $i \in \mathcal{N}^{\mathrm{MT}}$ are given as follows.

$$0 \leq P_{i,s,t} \leq \bar{P}_i^{\mathrm{MT}} \tag{10a}$$

$$P_i^{\mathrm{MT,rd}} \leq P_{i,s,t+1} - P_{i,s,t} \leq P_i^{\mathrm{MT,ru}}, \ \forall t \in \mathcal{T} \setminus \{T\} \tag{10b}$$

5) LOAD SERVING CONSTRAINTS

For each load at node $i \in \mathcal{N}^{\mathrm{L}}$, the variable α^{ls} is the ratio of the served load to the actual load demand. With a constant power factor at all load buses, the condition is expressed as

$$0 \leq \alpha_{i,s,t}^{\mathrm{ls}} = \frac{P_{i,s,t}}{P_{i,s,t}^{\mathrm{L}}} = \frac{Q_{i,s,t}}{Q_{i,s,t}^{\mathrm{L}}} \leq 1. \tag{11}$$

6) STATIC ENERGY STORAGE CONSTRAINTS

In order to have fast responses with high ramping rates, static energy storage systems or ES units are used as an alternative to traditional spinning reserves, which comes into effect immediately after a power outage. For every ES unit $i \in \mathcal{N}^{\mathrm{ES}}$, we have the following constraints. (12a) is the dynamic equation of the state of charge (SoC)S^{S} with the amounts of charging and discharging power $\{P^{\mathrm{ES,ch}}, P^{\mathrm{ES,dis}}\}$, which are associated with the efficiency factors $\{\eta^{\mathrm{ch}}, \eta^{\mathrm{dis}}\}$. The initial SoC, and lower/upper limits for all the ES units are specified in (12b). (12c) ensures the charging and discharging status with the appropriate upper limit. In order to limit the use of mixed integer variables, the complementarity constraint is formulated as specified in (12d). Finally, (12e) gives the net real power injection at any ES bus.

$$S_{i,s,t+1}^{\mathrm{S}} = S_{i,s,t}^{\mathrm{S}} + \eta^{\mathrm{ch}}\Delta t P_{i,s,t}^{\mathrm{ES,ch}} - \frac{1}{\eta^{\mathrm{dis}}}\Delta t P_{i,s,t}^{\mathrm{ES,dis}},$$
$$\forall t \in \mathcal{T} \setminus \{T\} \tag{12a}$$

$$S_{i,s,1}^{\mathrm{S}} = S_{i,s}^{\mathrm{S,int}}, \quad \underline{S} \leq S_{i,s,t}^{\mathrm{S,int}} \leq \bar{S} \tag{12b}$$

$$0 \leq P_{i,s,t}^{\mathrm{ES,ch}} \leq \bar{P}_i^{\mathrm{ES,ch}}, 0 \leq P_{i,s,t}^{\mathrm{ES,dis}} \leq \bar{P}_i^{\mathrm{ES,dis}} \tag{12c}$$

$$P_{i,s,t}^{\mathrm{ES,ch}} \times P_{i,s,t}^{\mathrm{ES,dis}} = 0 \tag{12d}$$

$$P_{i,s,t} = P_{i,s,t}^{\mathrm{ES,dis}} - P_{i,s,t}^{\mathrm{ES,ch}}. \tag{12e}$$

7) MOBILE ENERGY STORAGE CONSTRAINTS

The MS units follow the same operating principle as ES. (13a)-(13c) denote the SoC constraints and net real power injections. Coupling constraints (13d) and (13e) respectively denote the charging and discharging power limit where an MS unit is sited. These units can either be charged, discharged or remain idle at any time as specified by the binary indicators

α^{ch} and α^{dis} in (13f).

$$S^{\text{M}}_{i,s,t+1} = S^{\text{M}}_{i,s,t} + \eta^{\text{ch}}\Delta t P^{\text{MS,ch}}_{i,s,t} - \frac{1}{\eta^{\text{dis}}}\Delta t P^{\text{MS,dis}}_{i,s,t},$$

$$\forall t \in \mathcal{T} \setminus \{T\} \tag{13a}$$

$$S^{\text{M}}_{i,s,1} = S^{\text{M,int}}_{i,s}, \quad \underline{S} \le S^{\text{M}}_{i,s,t} \le \bar{S} \tag{13b}$$

$$P_{i,s,t} = P^{\text{MS,dis}}_{i,s,t} - P^{\text{MS,ch}}_{i,s,t}. \tag{13c}$$

$$0 \le P^{\text{MS,ch}}_{i,s,t} \le Z_i \times \alpha^{\text{ch}}_{i,s,t} \times \bar{P}^{\text{MS,ch}}_i \tag{13d}$$

$$0 \le P^{\text{MS,dis}}_{i,s,t} \le Z_i \times \alpha^{\text{dis}}_{i,s,t} \times \bar{P}^{\text{MS,dis}}_i \tag{13e}$$

$$\alpha^{\text{ch}}_{i,s,t} + \alpha^{\text{dis}}_{i,s,t} \le 1 \tag{13f}$$

D. OPTIMIZATION PROBLEM AND CONVEXIFICATION

To this end, we formulate the following stochastic OPF problem for the MG facing a progressing wildfire.

$$\underset{\mathcal{V}_1,\mathcal{V}_2,\mathcal{V}^{\text{DLR}}}{\text{minimize}} \quad C_1(\mathcal{V}_1) + C_2(\mathcal{V}_2)$$

$$\text{subject to } (2), (6) - (13). \tag{14}$$

The optimization variables $\mathcal{V}_1 \triangleq \{X_i, Z_j\}_{i\in\mathcal{N}^{\text{QS}}, j\in\mathcal{N}\setminus\mathcal{N}^{\text{L}}, t\in\mathcal{T}}$ and $\mathcal{V}_2 \triangleq \{\mathcal{V}^{\text{MT}}, \mathcal{V}^{\text{QS}}, \mathcal{V}^{\text{B}}, \mathcal{V}^{\text{NC}}, \mathcal{V}^{\text{ES}}, \mathcal{V}^{\text{MS}}, \mathcal{V}^{\text{L}}, \mathcal{V}^{\text{DLR}}\}$ are defined as follows.

$$\mathcal{V}^{\text{MT}} \triangleq \{P_{i,s,t}, Q_{i,s,t}\}_{i\in\mathcal{N}^{\text{MT}}, s\in\mathcal{S}, t\in\mathcal{T}}$$

$$\mathcal{V}^{\text{QS}} \triangleq \{P_{i,s,t}, Q_{i,s,t}, Y_{i,s,t}\}_{i\in\mathcal{N}^{\text{QS}}, s\in\mathcal{S}, t\in\mathcal{T}}$$

$$\mathcal{V}^{\text{B}} \triangleq \{\ell_{ij,s,t}, P_{ij,s,t}, Q_{ij,s,t}\}_{(i,j)\in\mathcal{E}, s\in\mathcal{S}, t\in\mathcal{T}}$$

$$\mathcal{V}^{\text{NC}} \triangleq \{v_{i,s,t}\}_{i\in\mathcal{N}, s\in\mathcal{S}, t\in\mathcal{T}}$$

$$\mathcal{V}^{\text{ES}} \triangleq \{P^{\text{ES,ch}}_{i,s,t}, P^{\text{ES,dis}}_{i,s,t}, S^{\text{S}}_{i,s,t}, P_{i,s,t}\}_{i\in\mathcal{N}^{\text{ES}}, s\in\mathcal{S}, t\in\mathcal{T}}$$

$$\mathcal{V}^{\text{MS}} \triangleq$$

$$\{P^{\text{MS,ch}}_{i,s,t}, P^{\text{MS,dis}}_{i,s,t}, S^{\text{M}}_{i,s,t}, P_{i,s,t}, \alpha^{\text{ch}}_{i,s,t}, \alpha^{\text{dis}}_{i,s,t}\}_{i\in\mathcal{N}^{\text{MS}}, s\in\mathcal{S}, t\in\mathcal{T}}$$

$$\mathcal{V}^{\text{L}} \triangleq \{\alpha^{\text{ls}}_{i,s,t}\}_{i\in\mathcal{N}^{\text{L}}, s\in\mathcal{S}, t\in\mathcal{T}}$$

$$\mathcal{V}^{\text{DLR}} \triangleq \{T_{ij,s,t}, u_{ij,s,t}, \ell_{ij,s,t}\}_{s\in\mathcal{S}, t\in\mathcal{T}}$$

It can be seen that the resulting problem (14) is highly nonconvex due to (2e), (2f), (7d), (9b), (12d), (13d) and (13e). Among them (7d) is relaxed to second order cone constraints [48]. (12c)-(12e) is replaced with the convex hull of its non-convex feasible region. The closed form of which is given as [48].

$$P^{\text{ES,ch}}_{i,s,t} \ge 0 \tag{15a}$$

$$P^{\text{ES,dis}}_{i,s,t} \ge 0 \tag{15b}$$

$$\frac{P^{\text{ES,ch}}_{i,s,t}}{\bar{P}^{\text{ES,ch}}_i} + \frac{P^{\text{ES,dis}}_{i,s,t}}{\bar{P}^{\text{ES,dis}}_i} \le 1 \tag{15c}$$

We have bilinear terms in (13d) and (13e). To convexify, we introduce two new sets of binary variables τ^{ch} and τ^{dis} and replace the said equations as follows.

$$\tau^{\text{ch}}_{i,s,t} \le Z_i, \quad \tau^{\text{dis}}_{i,s,t} \le Z_i \tag{16a}$$

$$\tau^{\text{ch}}_{i,s,t} \le \alpha^{\text{ch}}_{i,s,t}, \quad \tau^{\text{dis}}_{i,s,t} \le \alpha^{\text{dis}}_{i,s,t} \tag{16b}$$

$$\tau^{\text{ch}}_{i,s,t} \ge \left(Z_i + \alpha^{\text{ch}}_{i,s,t} - 1\right), \tau^{\text{dis}}_{i,s,t} \ge \left(Z_i + \alpha^{\text{dis}}_{i,s,t} - 1\right) \tag{16c}$$

$$0 \le P^{\text{MS,ch}}_{i,s,t} \le \tau^{\text{ch}}_{i,s,t} \times \bar{P}^{\text{MS,ch}}_i \tag{16d}$$

$$0 \le P^{\text{MS,dis}}_{i,s,t} \le \tau^{\text{dis}}_{i,s,t} \times \bar{P}^{\text{MS,dis}}_i \tag{16e}$$

For handling the non-convexity in (2e) and (2f), [8], uses a simple linearization technique as shown in (17a)-(17b). Specifically, by fixing the line temperature at its maximum allowable value $\bar{T}^{ij}$, the outer approximation (17a) acts as a surrogate for the resistive heat gain (2e). Regarding the radiative heat loss (2f), it is linearized with respect to the line temperature as shown in (17b).

$$q^{\text{l}}_{ij,s,t} \ge R_{ij,s,t}(\bar{T}^{ij}) \times \ell_{ij}, s, t \tag{17a}$$

$$q^{\text{r}}_{ij,s,t} = \lambda^{\text{r}} \times T_{ij,s,t} + \beta^{\text{r}}. \tag{17b}$$

By using these approximations, (2) becomes a set of linear equality and inequality constraints in $\mathcal{V}^{\text{DLR}}$, which results in a mixed-integer second-order cone program.

In this work, we observe the fact that the resistive heat gain $q^{\text{l}}_{ij,s,t}$ contributes much less to the line temperature change, compared with all other heat sources in (2a). Therefore, when dealing with the bilinear term $\ell_{ij,s,t} \times T_{ij,s,t}$ in (2e), we fix the line current at its upper limit. Consequently, the resistive heat gain $q^{\text{l}}_{ij,s,t}$ becomes a linear function in line temperature only, as given below.

$$q^{\text{l}}_{ij,s,t} = R_{ij,s,t}(T_{ij,s,t}) \times \bar{\ell}^{ij}. \tag{18}$$

Remark 1: The advantage of our proposed approximation is threefold. First and foremost, detaching the DLR constraints helps in shrinking the set of decision variables by cutting off the squared magnitude of current, $\ell_{ij,s,t}$ and the line outage indicator, $u_{ij,s,t}$ from the main optimization problem. As $u_{ij,s,t}$ can be obtained by solving (2) independently, the computational time gets reduced to one-tenth according to our simulation. Therefore, we can afford to include more practical constraints in the optimization problem. Second, separating DLR also frees the line temperature T_{ij} from being a decision variable. Hence, we do not need to make any strong assumption to linearize the quartic function in equation (2f) unlike some traditional approaches [8], [9]. We can keep it intact without increasing the degree of complexity as it is solved outside the main optimization problem. This helps us to avoid any unnecessary approximation errors. Third, $u_{ij,s,t}$ no more being a decision variable intrinsically solves the non-convexity in (9b).

Finally, we illustrate the overall scheme of the proposed framework in Figure 1. Derived from the scenario generation, binary indicator u_{ij}, renewable power generation P^{PV}, P^{WT}, as well as the load demand P^{L} are provided as the optimization problem inputs.

IV. SIMULATION RESULTS

In this section, we present extensive simulation results to show the merits of our proposed framework.

A. SIMULATION SETUP

All the simulations are carried out in a PC with Intel Core i7, 3.6 GHz CPU and 32GB RAM. A modified IEEE 22-bus
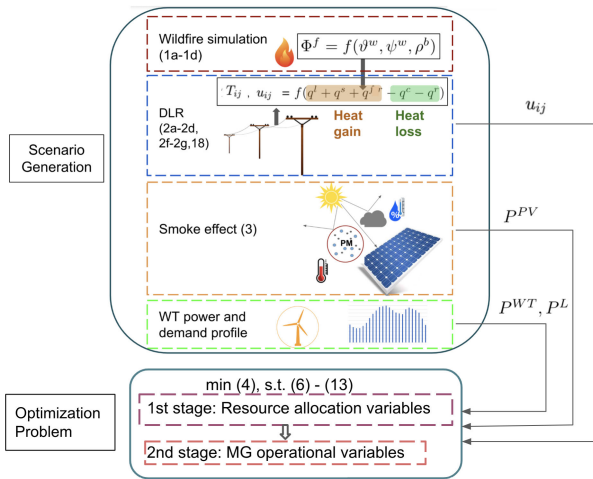
FIGURE 1. Framework of our proposed model: the generated renewable power, load demand and tie line outage status serve as the inputs of the resulting optimization problem from which the DLR constraints are separated.
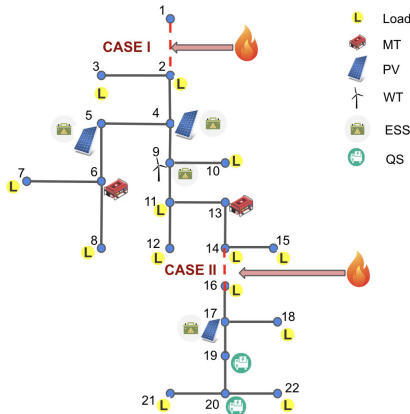

FIGURE 2. Outage lines and DER in the simulated system.

distribution system is used which has 3 PV units, 1 WT, 2 MT, and 2 QS generators. An ES is installed with each of the renewable units. We consider two different cases of line outage. Case I represents a line outage between buses 1 and 2 while case II is between buses 14 and 15 as specified in figure 2. The network parameters are listed in Table 2. The demand profile data are collected from [49]. To focus on the smoke effect on PV generation, we run the simulations for daytime from 7 am until 9 pm. We generate 50 scenarios and use one of them to show the scheduling results by the figures in Section IV-D. We use Gurobi 9.3 [50] along with CVX [51] to solve the resulting SOCP.

B. WILDFIRE SIMULATION AND DLR EFFECT

The parameters of the active wildfire simulation are given in Table 3. Based on our simulation, any power line is out of service when the line conductor temperature T_{ij} exceeds 350 K. We evaluate the effect of separating the DLR constraints from the optimization problem by checking the

TABLE 2. Values of the network parameters.

Parameter	Value
$\mathcal{N}^{\mathrm{L}}$	{2,3,7,8,10,11,12,14,15,16,18,21,22}
β	2, 2, 3, 4, 8, 3, 3, 8, 9, 2, 11, 12, 7
T, T' Δt	15, 4, 1hr
$\gamma^{\mathrm{B}}, \gamma^{\mathrm{S}}, \gamma^{\mathrm{RF}}, \gamma^{\mathrm{QS}}, \gamma^{\mathrm{MT}}, \gamma^{\mathrm{L}}$	50, 50, 200, 65, 70, 10000
$\underline{v}, \bar{v}$	0.95, 1.05
$\bar{P}^{\mathrm{MT}}, P^{\mathrm{MT,ru}}, P^{\mathrm{MT,rd}}$	0.05, 0.03, -0.02
$\bar{Y}^{\delta}, \underline{Y}^{\delta}, \eta^{\mathrm{QS}}$	{0.06, 0.07}, {0.025, 0.03}, 0.6
$\eta^{\mathrm{dis}}, \eta^{\mathrm{ch}}, S^{\mathrm{int}}$	0.9, 0.9, 0.4
$\bar{P}^{\mathrm{ES,dis}}$	{0.0328, 0.03, 0.0315, 0.0290}
$\bar{P}^{\mathrm{ES,ch}}$	{0.0308, 0.0208, 0.0280, 0.350}
$\bar{P}^{\mathrm{MS,dis}}$	{0.0197, 0.018, 0.0189, 0.0174}
$\bar{P}^{\mathrm{MS,ch}}$	{0.0185, 0.0125, 0.0168, 0.210}

TABLE 3. Parameters of the wildfire simulation.

Parameter	Value
$\rho^{\mathrm{b}}, H, \varphi$	40, 15, 200
$\tau^{\mathrm{a}}, \sigma^{\mathrm{f}}, \kappa_{\mathrm{B}}, T_{\mathrm{f}}$	1, 1, 5.67×10^{-8}, 1400
$\varrho, \epsilon, \zeta, \sigma^{\mathrm{c}}$	2.1×10^{-2}, 18, 4.04×10^{-3}, 0.78
$R_{ij,ref}, T_{ij,ref}, \bar{T}_{ij}$	15, 293, 350
$\mu^{\mathrm{a}}, \rho^{\mathrm{a}}, \kappa^{\mathrm{a}}$	2.624×10^{-2}, 1.184, 1.849×10^{-5}

TABLE 4. The PMAD of the tie line outage indicator including vs excluding DLR in the optimization problem.

N_s	10	25	40	50
PMAD	4%	3.2%	2.8%	2.6%

change of the binary indicator variables. Let u^{inc} denote the optimal solution of the line outage indicator to the problem (14) with DLR. In contrast, u^{exc} is the counterpart obtained by independently solving (2), where (2e) is replaced by (18). The performance metric is the percentage of the mean absolute difference (PMAD) defined as

$$\mathrm{PMAD} = \frac{1}{N_s T} \sum_{s=1}^{N_s} \sum_{t=1}^{T} \left| u_{s,t}^{\mathrm{inc}} - u_{s,t}^{\mathrm{exc}} \right| \times 100\%.$$

As we can see in Table 4, the difference is quite small, which decreases with the increased number of scenarios. Thus, this result corroborates the validity of our proposed method.

Table 5 compares the effect of fire spreading factors on load shedding. Factors working against fire growth postpone the line outage time which reduces the amount of load curtailment. The numbers in the table corroborate this fact. With higher level of firefighting efforts (F), the load shedding is less. Similarly, the presence of a water body or similar structure and downhill topography reduces the curtailed load.

C. SMOKE EFFECT ON PV GENERATION

The PV output data of the Bennion Creek fire in Utah were collected from [52]. The PM2.5 and PM10 data for the same location are from [53] while the other meteorological data can be found in [54]. Based on this data set, the optimal coefficients of the regression model (3) are given in Table 6. Clearly, DNI is a leading factor that contributes the most to the PV output, while temperature also has a positive correlation.

TABLE 5. Effects of fire spreading factors in load curtailment.

Factors	Value	Curtailed load (MW)
Human intervention (F)	0 (null effort)	2.908
	0.6 (moderate)	2.075
	0.9 (extensive)	1.615
Natural obstacle (N)	0 (not existing)	2.88
	1.2 (existing)	0.53
Topography (M)	0 (uphill)	2.469
	1 (downhill)	1.83

TABLE 6. Learned coefficients of the features for the smoke effect.

Variable	Coefficient
Constant term	$\alpha_0 = 47.102$
Temperature (Z_1)	$\alpha_1 = 27.9705$
Relative humidity (Z_2)	$\alpha_2 = -4.832$
DNI (Z_3)	$\alpha_4 = 32.377$
Cloud opacity (Z_4)	$\alpha_4 = -2.037$
PM2.5 (Z_5)	$\alpha_5 = -0.603$
PM10 (Z_6)	$\alpha_6 = -7.857$

Other features including relative humidity, cloud opacity, PM2.5 and PM10 are all negatively correlated with the response indicating the inverse relationship. This regression result confirms our intuition of how those features affect the PV generation.

D. MG OPERATION

Figure 3 to figure 7 are carried down for case I, with moderate firefighting effort, without any natural obstacle and a flat landscape. Figure 3 shows the fuel consumption profile for the two QS units. As we can see in the figure, before the line outage takes place at 1 pm, the fuel levels remain the same as their initially allocated amounts (cf. Table 7). Then, the QS generators start consuming fuels to support the load demand from 2 pm.

Figure 4 shows the charging and discharging power scheduling of all four ES and three MS units. The ES units keep charging before islanding and discharging afterward to prioritize load serving. As the MS units were fully charged at the time of siting, hence they start discharging as soon as the line gets tripped off. Clearly, the limits of charging/discharging power and SoC are always respected during the entire time horizon.

Three MS units are sited at bus 4,5 and 9. Table 8 shows that without allocating these resources, the total amount of load shed is higher than having them at the designated buses.

Figure 5 depicts the real power generated by the two MTs. Before islanding, the MG mainly relies on purchased power from the upstream grid, which is cheaper than utilizing the MT units. Hence, the initial power generation of these units is low. After the tie line outage, the MTs ramp up their generation to support the critical loads in the absence of upstream power.

Figure 6 shows the load serving status of each bus prioritizing the critical loads. The color gradient indicates the fraction of the picked-up demand α^{ls}. According to
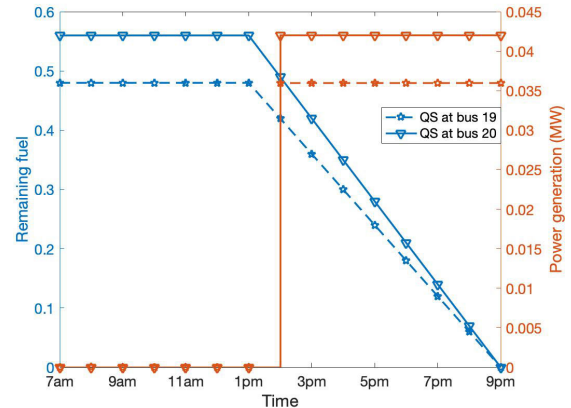

FIGURE 3. Fuel expenditure profiles for the QS units.

TABLE 7. Fuel allocation for QS units.

	Without smoke effect		With smoke effect	
Allocated fuels	QS unit 1	QS unit 2	QS unit 1	QS unit 2
X_i	0.4000	0.4400	0.4799	0.5599

the criticality factor given in Table 2, the least critical loads are located at bus 2, 3, 7, 8, 11, 12 and 16. Hence, they are shed as soon as the MG gets islanded and all other loads are instantly supported by the distributed resources. Then, the higher priority loads among them i.e. 7 and 8 are gradually picked up by the QS units.

To show the effectiveness of our proposed approach, we compare it with two other cases. Case A is MG operation without considering the smoke effect. Case B is the one including the smoke effect but no provision of QS units. case C is our proposed one (including both smoke effect and QS units). Figure 7 displays the benefit of incorporating the smoke effect. Without considering the smoke effect, the PV generation is simply over-estimated and hence less amount of reserves are bought (cf. Table 7). The reserves are not sufficient enough to compensate the shortened generation under an actual smoky scenario. In Figure 7, it is demonstrated that the total amount of load shedding is higher in such a case. The maximum amount of load shedding occurs right at 1 pm when the islanding happens. From 2 pm, the QS units start reducing the amount of unserved loads. Clearly, there is no load shedding for the first 6 hours since all MG loads can be supported by the power from the upstream grid.

To compare cases B and C, we calculate the total generation cost and load shedding cost with and without the QS units. Note that, both of these cases consider the smoke effect. According to Table 9, the generation cost in our proposed method (case C) is higher because it involves both MT and QS units. However, in case B we have to shed lots of load due to insufficient generation. This inevitably increases the total cost.

Now, we consider another case (case II) where a leftward fire affects the line connecting bus 14 and 16, see figure 2. The load serving status is shown in figure 8. Bus 16,18,21
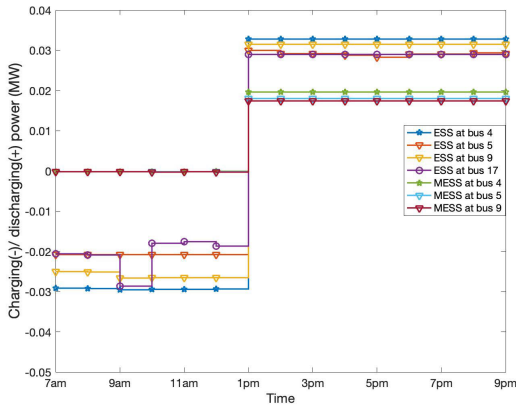
FIGURE 4. Optimal scheduling of ES and MS charging/discharging power.

TABLE 8. Impact of allocating MS units.

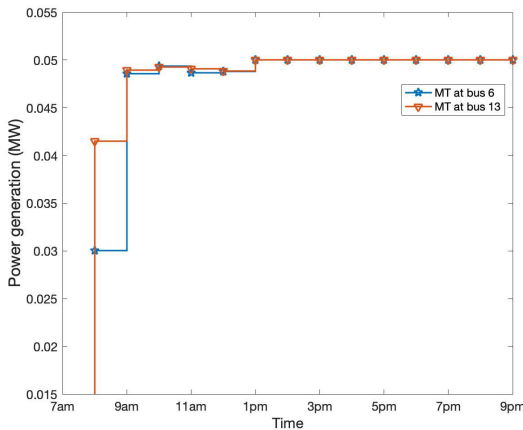| Sited bus index	Load shed with MS	Load shed w/o MS
4, 5, 9	2.075 (MW)	2.5694 (MW)

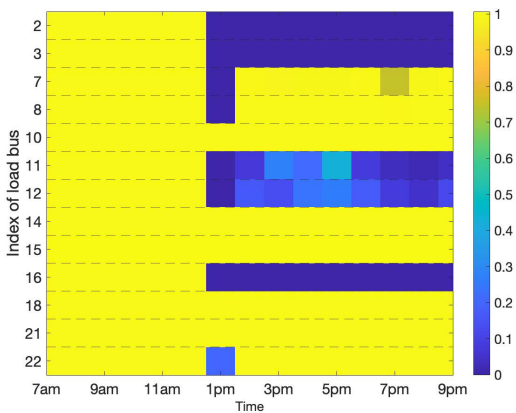**FIGURE 5.** Optimal real power generation by the MTs.

FIGURE 6. Serving status (α^{ls}) of each load bus for case I.

and 22 are disconnected from the upper sub-network (bus 1 to bus 15). In the lower network, the lowest priority load at bus 22 gets curtailed due to insufficient resources. On the other hand, resources in the upper network can be fully utilized to serve comparatively low priority loads (load at
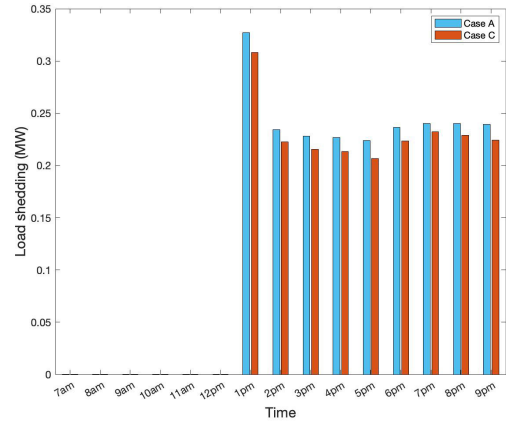
FIGURE 7. Total amount of load shedding considering smoke effect (Case C) and without considering smoke effect (Case A).

TABLE 9. The cost comparison between case B and C (unit in $).

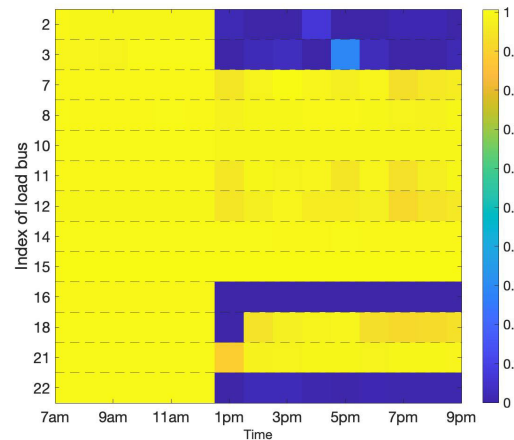| Type of cost	Case B	Case C
MT generation cost	$96.6531	$96.6531
QS generation cost	–	$248.5596
Load shedding cost	$72,507.67	$48,079.80
Total cost	$72,604.32	$48,425.01

FIGURE 8. Serving status (α^{ls}) of each load bus for case II.

bus 11 and 12) which was unserved in case I. Table 10 shows that the total load shed amount is lower with a higher generation cost in case I while case II experiences the opposite.

Figure 9 demonstrates the comparison of total load shedding between an in-sample and an out-of-sample scenario. Depending on the variation of renewable generation and active power demand, the amount of unserved load sometimes exceeds the in-sample case, and sometimes remains lower. Nevertheless, the difference in any time step is not too big, which shows the robustness of the optimal solution to our two-stage stochastic program.

Finally, Table 11 lists the optimal objective values and the computation time for solving the stochastic program. With the increased number of scenarios, the probability of simulating

TABLE 10. Comparison between different line outages.

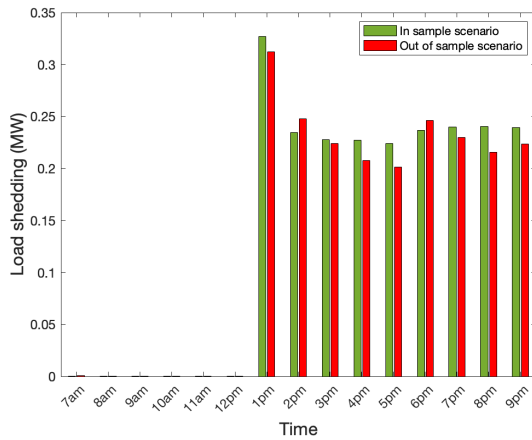| Criterion	Case I	Case II
Buses between the outaged lines	1, 2	14, 16
Total load shed (MW)	2.075	2.163
Generation cost ($)	345.21	325.96

FIGURE 9. The comparison of load shedding in-sample and out-of-sample cases.

TABLE 11. Comparison among different number of scenarios.

Number of scenarios	Optimal value $(\times 10^3)$	Computation time (sec)
10	-478.593	204.30
25	-465.672	678.98
40	-466.566	1432.87
50	-465.789	2550.567

the actual scenario gets higher. By trading off between the computation time and optimality, we choose 50 as the number of scenarios.

V. CONCLUSION

In this work, we formulate a two-stage stochastic OPF in the context of operating a MG during a wildfire. A comprehensive model of fire dynamics causing line outage and altered PV generation stemming from the smoke plume is analyzed. In order to prepare for the upcoming contingency more accurately while minimizing load shedding, we exploit renewable fuel driven quick start generators and mobile energy storage devices. One of the biggest advantages of our proposed framework is making the computation much faster by efficiently detaching the DLR constraints from the OPF problem. The extensive simulations demonstrate the merit of the proposed model by comparing the power outage and operational costs in various case studies. Without considering the smoke effect, PV generation is always overestimated, which results in higher load shedding and affecting the resiliency of the system. In future, we plan to utilize advanced sensors and communication system to characterize the uncertainties in fire progression more precisely. Moreover, the inclusion of wind propagation factor can aid in a better modelling of smoke effect in real PV generation. Another

interesting direction is to leverage clean energy technologies that helps in making the grid more sustainable and resilient.

REFERENCES

[1] A. Lindstrom and S. Hoff, "US electricity customers experienced eight hours of power interruptions in 2020," in *Proc. Annu. Elect. Power Ind. Rep.*, Nov. 2021. [Online]. Available: https://www.eia.gov/todayinenergy/detail.php?id=50316

[2] S. Kirshenberg, H. Jackler, J. Eun, B. Oakley, and W. Goldenberg, "Small modular reactors: Adding to resilience at federal facilities," U.S. Dept. Energy (DOE), Washington, DC, USA, Tech. Rep. DOE0638-1022-11, 2017.

[3] S. York, "Smoke from California wildfires decreases solar generation in CAISO," U.S. Energy Inf. Admin., Washington, DC, USA, Tech. Rep., Sep. 2020.

[4] S. Chowdhury, K. Zhu, and Y. Zhang, "Mitigating greenhouse gas emissions through generative adversarial networks based wildfire prediction," 2021, *arXiv:2108.08952*.

[5] Z. Xiaozhi, L. Tao, X. Kan, C. Zhiguo, C. Xiaoming, and R. Ling, "Evaluation of wildfire occurrence along high voltage power line by remote sensing data: A case study in Xianning, Hubei, China," in *Proc. 4th Int. Workshop Earth Observ. Remote Sens. Appl. (EORSA)*, Jul. 2016, pp. 300–304.

[6] P. Yang, T. Spencer, C. Stripling, D. Shoemate, and N. R. Modala, "Reinforcing wildfire predictive services with timely weather information," in *Proc. 25th Int. Conf. Geoinformatics*, Aug. 2017, pp. 1–4.

[7] H. Liang, M. Zhang, and H. Wang, "A neural network model for wildfire scale prediction using meteorological factors," *IEEE Access*, vol. 7, pp. 176746–176755, 2019.

[8] D. N. Trakas and N. D. Hatziargyriou, "Optimal distribution system operation for enhancing resilience against wildfires," *IEEE Trans. Power Syst.*, vol. 33, no. 2, pp. 2260–2271, Mar. 2018.

[9] S. Mohagheghi and S. Rebennack, "Optimal resilient power grid operation during the course of a progressing wildfire," *Int. J. Electr. Power Energy Syst.*, vol. 73, pp. 843–852, Dec. 2015.

[10] M. Nazemi and P. Dehghanian, "Powering through wildfires: An integrated solution for enhanced safety and resilience in power grids," *IEEE Trans. Ind. Appl.*, vol. 58, no. 3, pp. 4192–4202, May 2022.

[11] S. Dian, P. Cheng, Q. Ye, J. Wu, R. Luo, C. Wang, D. Hui, N. Zhou, D. Zou, Q. Yu, and X. Gong, "Integrating wildfires propagation prediction into early warning of electrical transmission line outages," *IEEE Access*, vol. 7, pp. 27586–27603, 2019.

[12] A. Arif, S. Ma, Z. Wang, J. Wang, S. M. Ryan, and C. Chen, "Optimizing service restoration in distribution systems with uncertain repair time and demand," *IEEE Trans. Power Syst.*, vol. 33, no. 6, pp. 6828–6838, Nov. 2018.

[13] H. Farzin, M. Fotuhi-Firuzabad, and M. Moeini-Aghtaie, "Stochastic energy management of microgrids during unscheduled islanding period," *IEEE Trans. Ind. Informat.*, vol. 13, no. 3, pp. 1079–1087, Jun. 2017.

[14] J. Lee, S. Lee, and K. Lee, "Multistage stochastic optimization for microgrid operation under islanding uncertainty," *IEEE Trans. Smart Grid*, vol. 12, no. 1, pp. 56–66, Jan. 2021.

[15] A. Zakaria, F. B. Ismail, M. S. H. Lipu, and M. A. Hannan, "Uncertainty models for stochastic optimization in renewable energy applications," *Renew. Energy*, vol. 145, pp. 1543–1571, Jan. 2020.

[16] T. Tapia, Á. Lorca, D. Olivares, M. Negrete-Pincetic, and A. J. Lamadrid, "A robust decision-support method based on optimization and simulation for wildfire resilience in highly renewable power systems," *Eur. J. Oper. Res.*, vol. 294, no. 2, pp. 723–733, Oct. 2021.

[17] E. Craparo, M. Karatas, and D. I. Singham, "A robust optimization approach to hybrid microgrid operation using ensemble weather forecasts," *Appl. Energy*, vol. 201, pp. 135–147, Sep. 2017.

[18] H. Shuai, J. Fang, X. Ai, Y. Tang, J. Wen, and H. He, "Stochastic optimization of economic dispatch for microgrid based on approximate dynamic programming," *IEEE Trans. Smart Grid*, vol. 10, no. 3, pp. 2440–2452, May 2019.

[19] E. Grover-Silva, M. Heleno, S. Mashayekh, G. Cardoso, R. Girard, and G. Kariniotakis, "A stochastic optimal power flow for scheduling flexible resources in microgrids operation," *Appl. Energy*, vol. 229, pp. 201–208, Nov. 2018.

[20] A. R. Malekpour and A. Pahwa, "Stochastic networked microgrid energy management with correlated wind generators," *IEEE Trans. Power Syst.*, vol. 32, no. 5, pp. 3681–3693, Sep. 2017.

[21] D. Wang, J. Qiu, L. Reedman, K. Meng, and L. L. Lai, "Two-stage energy management for networked microgrids with high renewable penetration," *Appl. Energy*, vol. 226, pp. 39–48, Sep. 2018.

[22] A. Bagheri, C. Zhao, F. Qiu, and J. Wang, "Resilient transmission hardening planning in a high renewable penetration era," *IEEE Trans. Power Syst.*, vol. 34, no. 2, pp. 873–882, Mar. 2019.

[23] A. Gholami, T. Shekari, and S. Grijalva, "Proactive management of microgrids for resiliency enhancement: An adaptive robust approach," *IEEE Trans. Sustain. Energy*, vol. 10, no. 1, pp. 470–480, Jan. 2019.

[24] J. Son, S. Jeong, H. Park, and C.-E. Park, "The effect of particulate matter on solar photovoltaic power generation over the republic of Korea," *Environ. Res. Lett.*, vol. 15, no. 8, Aug. 2020, Art. no. 084004.

[25] L. Yu, M. Zhang, L. Wang, Y. Lu, and J. Li, "Effects of aerosols and water vapour on spatial-temporal variations of the clear-sky surface solar radiation in China," *Atmos. Res.*, vol. 248, Jan. 2021, Art. no. 105162.

[26] A. J. Ali, L. Zhao, and M. H. Kapourchali, "Data-driven-based analysis and modeling for the impact of wildfire smoke on PV systems," *IEEE Trans. Ind. Appl.*, vol. 60, pp. 1–10, 2023.

[27] A. J. Ali, L. Zhao, M. H. Kapourchali, and W.-J. Lee, "Development of a quantification method for the impact of wildfire smoke on photovoltaic systems," in *Proc. IEEE/IAS 59th Ind. Commercial Power Syst. Tech. Conf. (I&CPS)*, 2023, pp. 1–10.

[28] A. J. Ali, L. Zhao, M. H. Kapourchali, and W.-J. Lee, "The wiggle effect of wildfire smoke on PV systems and frequency stability analysis for low-inertia power grids," in *Proc. IEEE/IAS 59th Ind. Commercial Power Syst. Tech. Conf. (I&CPS)*, May 2023, pp. 1–8.

[29] N. Rhodes, L. Ntaimo, and L. Roald, "Balancing wildfire risk and power outages through optimized power shut-offs," *IEEE Trans. Power Syst.*, vol. 36, no. 4, pp. 3118–3128, Jul. 2021.

[30] R. Bayani and S. D. Manshadi, "Resilient expansion planning of electricity grid under prolonged wildfire risk," *IEEE Trans. Smart Grid*, vol. 14, no. 5, pp. 3719–3731, Sep. 2023.

[31] X. Zhu, B. Zeng, Y. Li, and J. Liu, "Co-optimization of supply and demand resources for load restoration of distribution system under extreme weather," *IEEE Access*, vol. 9, pp. 122907–122923, 2021.

[32] X. Wang, X. Wang, Y. Zhang, Y. Liu, Y. Duan, and D. D. Micu, "Enhancing resilience of distribution systems considering electric vehicles and network reconfiguration in post-extreme events," in *Proc. 10th Int. Conf. Modern Power Syst. (MPS)*, Jun. 2023, pp. 01–06.

[33] A. Arif, Z. Wang, C. Chen, and J. Wang, "Repair and resource scheduling in unbalanced distribution systems using neighborhood search," *IEEE Trans. Smart Grid*, vol. 11, no. 1, pp. 673–685, Jan. 2020.

[34] S. Poudel and A. Dubey, "Critical load restoration using distributed energy resources for resilient power distribution system," *IEEE Trans. Power Syst.*, vol. 34, no. 1, pp. 52–63, Jan. 2019.

[35] Q. Zhang, Z. Wang, S. Ma, and A. Arif, "Stochastic pre-event preparation for enhancing resilience of distribution systems," *Renew. Sustain. Energy Rev.*, vol. 152, Dec. 2021, Art. no. 111636.

[36] L. Che and M. Shahidehpour, "Adaptive formation of microgrids with mobile emergency resources for critical service restoration in extreme conditions," *IEEE Trans. Power Syst.*, vol. 34, no. 1, pp. 742–753, Jan. 2019.

[37] S. Cai, Y. Xie, Q. Wu, M. Zhang, X. Jin, and Z. Xiang, "Distributionally robust microgrid formation approach for service restoration under random contingency," *IEEE Trans. Smart Grid*, vol. 12, no. 6, pp. 4926–4937, Nov. 2021.

[38] Y. Liu, Z. Tang, and L. Wu, "On secured spinning reserve deployment of energy-limited resources against contingencies," *IEEE Trans. Power Syst.*, vol. 37, no. 1, pp. 518–529, Jan. 2022.

[39] Z. Li, C. Zang, P. Zeng, H. Yu, and H. Li, "Two-stage stochastic programming based model predictive control strategy for microgrid energy management under uncertainties," in *Proc. Int. Conf. Probabilistic Methods Appl. to Power Syst. (PMAPS)*, Oct. 2016, pp. 1–6.

[40] F. Garcia-Torres, C. Bordons, J. Tobajas, R. Real-Calvo, I. Santiago, and S. Grieu, "Stochastic optimization of microgrids with hybrid energy storage systems for grid flexibility services considering energy forecast uncertainties," *IEEE Trans. Power Syst.*, vol. 36, no. 6, pp. 5537–5547, Nov. 2021.

[41] L. P. Raghav, R. S. Kumar, D. K. Raju, and A. R. Singh, "Optimal energy management of microgrids using quantum teaching learning based algorithm," *IEEE Trans. Smart Grid*, vol. 12, no. 6, pp. 4834–4842, Nov. 2021.

[42] H. Zhao, H. Lu, B. Li, X. Wang, S. Zhang, and Y. Wang, "Stochastic optimization of microgrid participating day-ahead market operation strategy with consideration of energy storage system and demand response," *Energies*, vol. 13, no. 5, p. 1255, Mar. 2020.

[43] M. Perry and A. Troccoli, "Impact of a fire burn on solar irradiance and PV power," *Sol. Energy*, vol. 114, pp. 167–173, Apr. 2015.

[44] S. A. Arefifar, Y. A. I. Mohamed, and T. H. M. El-Fouly, "Supply-adequacy-based optimal construction of microgrids in smart distribution systems," *IEEE Trans. Smart Grid*, vol. 3, no. 3, pp. 1491–1502, Sep. 2012.

[45] J. L. Rossi, A. Simeoni, B. Moretti, and V. Leroy-Cancellieri, "An analytical model based on radiative heating for the determination of safety distances for wildland fires," *Fire Saf. J.*, vol. 46, no. 8, pp. 520–527, Nov. 2011.

[46] *IEEE Standard for Calculating the Current-Temperature Relationship of Bare Overhead Conductors*, IEEE Standard 738-2012, 2012, pp. 1–72.

[47] M. Farivar and S. H. Low, "Branch flow model: Relaxations and convexification—Part II," *IEEE Trans. Power Syst.*, vol. 28, no. 3, pp. 2565–2572, Aug. 2013.

[48] S. Bose and Y. Zhang, "Load restoration in islanded microgrids: Formulation and solution strategies," *IEEE Trans. Control Netw. Syst.*, pp. 1–12, 2024.

[49] *Electric Reliability Council of Texas (ERCOT)*. Accessed: Jan. 20, 2022. [Online]. Available: https://www.ercot.com/files/docs/2021/11/12/Native_Load_2021.zip

[50] Gurobi Optimization LLC. (2021). *Gurobi Optimizer Reference Manual*. [Online]. Available: https://www.gurobi.com

[51] M. Grant and S. Boyd. (Mar. 2014). *CVX: MATLAB Software for Disciplined Convex Programming, Version 2.1*. [Online]. Available: http://cvxr.com/cvx

[52] *A Year of Solar Data*. Accessed: Aug. 31, 2021. [Online]. Available: http://dvschroeder.blogspot.com/2016/09

[53] *Sensor Data Download Tool*. Accessed: Aug. 31, 2021. [Online]. Available: https://www.purpleair.com/sensorlist

[54] *The Solcast API Toolkit*. Accessed: Sep. 1, 2021. [Online]. Available: https://toolkit.solcast.com.au/
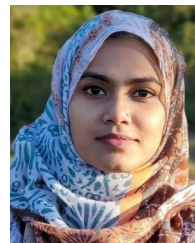
SIFAT CHOWDHURY received the B.S. degree in electrical and electronic engineering from Bangladesh University of Engineering and Technology (BUET) and the M.S. degree in electrical and computer engineering from the University of California, Santa Cruz. Her research interests include electric power system optimization, microgrid operation, data analytics, and enhancing grid resilience during extreme weather events.
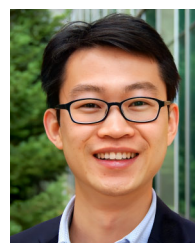
YU ZHANG (Member, IEEE) received the Ph.D. degree in electrical and computer engineering from the University of Minnesota, Minneapolis, MN, USA, in 2015. He is currently an Assistant Professor with the ECE Department, University of California at Santa Cruz (UCSC). Before joining UCSC, he held a postdoctoral position with the University of California at Berkeley and the Lawrence Berkeley National Laboratory. His research interests include cyber-physical systems, smart power grids, optimization theory, machine learning, and big data analytics. He was a recipient of the Hellman Fellowship, in 2019. He was a co-recipient of the Early Career Best Paper Award from the Energy, Natural Resources, and the Environment (ENRE) Section of the Institute of Operations Research and the Management Sciences (INFORMS), in 2021.

• • •